Organic & Biomolecular Chemistry

Cite this: *Org. Biomol. Chem.*, 2011, **9**, 5149

www.rsc.org/obc

PAPER

Absolute stereochemistry and preferred conformations of urate degradation intermediates from computed and experimental circular dichroism spectra†

Silvio Pipolo,‡[a] Riccardo Percudani[b] and Roberto Cammi*[a]

Received 18th March 2011, Accepted 19th April 2011
DOI: 10.1039/c1ob05433c

The enzymatic oxidation of urate leads to the sequential formation of optically active intermediates with unknown stereochemistry: (–)-5-hydroxyisourate (HIU) and (–)-2-oxo-4-hydroxy-4-carboxy-5-ureidoimidazoline (OHCU). In accordance with the observation that a defect in HIU hydrolase causes hepatocarcinoma in mouse, a detoxification role has been proposed for the enzymes accelerating the conversion of HIU and OHCU into optically active (+)-allantoin. The enzymatic products of urate oxidation are normally not present in humans, but are formed in patients treated with urate oxidase. We used time-dependent density functional theory (TDDFT) to compute the electronic circular dichroism (ECD) spectra of the chiral compounds of urate degradation (HIU, OHCU, allantoin) and we compared the results with experimentally measured ECD spectra. The calculated ECD spectra for (*S*)-HIU and (*S*)-OHCU reproduced well the experimental spectra obtained through the enzymatic degradation of urate. Less conclusive results were obtained with allantoin, although the computed optical rotations in the transparent region supported the original assignment of the (+)-*S* configuration. These absolute configuration assignments can facilitate the study of the enzymes involved in urate metabolism and help us to understand the mechanism leading to the toxicity of urate oxidation products.

1 Introduction

The assignment of the absolute configuration of chiral species involved in enzymatic reactions is essential for the understanding of biochemical processes. In this paper we present an experimental and computational study of the absolute configurations of intermediates involved in the enzymatic degradation of uric acid. Recent studies have been made on the purine degradation pathway (Scheme 1), supporting the presence of additional steps in the enzymatic conversion of uric acid (a purine derivative) to allantoin: oxidation of urate by the enzyme urate oxidase yields optically active 5-hydroxyisourate (HIU)*; the enzymatic or spontaneous hydrolysis of HIU yields optically active 2-oxo-4-hydroxy-4-carboxy-5-ureidoimidazoline (OHCU), an unstable intermediate that is converted into optically active allantoin by OHCU decarboxylase, or into racemic allantoin by spontaneous decay.[1]

The enzymatic pathway for the oxidative degradation of urate to allantoin occurs in bacteria, fungi, plants, and animals, including most mammals. Among mammals, notable exceptions are humans and apes. In these organisms the pathway is truncated due to inactivation of the three genes involved in urate catabolism (urate oxidase, HIU hydrolase, OHCU decarboxylase).[2] As a consequence, the levels of urate in human serum are tenfold higher than those in other primates. Uric acid is only marginally soluble, and its salt can precipitate in joints to cause gout and in the kidney to cause renal stones. An elective treatment for abnormally high levels of uric acid (hyperuricemia)—particularly for the surge of uric acid that characterizes the tumor lysis syndrome—is the intravenous administration of urate oxidase.[3] In normal conditions, small amounts of the urate oxidation products can be formed in humans by chemical oxidation. Following the urate oxidase treatment, however, the unstable intermediates of uric acid oxidation are formed in significant amounts in the patient's blood serum (the blood serum urate of patients subjected to the urate oxidase treatment can be as high as 14 mg dL^{-1}). In humans, the physiological consequences of the presence of such chemicals species are presently unknown, but recent studies in mouse indicate that HIU has strong toxic effects leading to hepatocarcinoma in the absence of a functioning HIU hydrolase.[4]

Complete information on the absolute configuration of the intermediates involved in the oxidation of the urate pathway is presently lacking. The absolute configuration for the allantoin

[a]*Dipartimento di Chimica "G.I.A.F", Universitá di Parma, 43100, Parma, Italy. E-mail: roberto.cammi@unipr.it; Fax: +39 0521905557; Tel: +39 0521905442*

[b]*Dipartimento di Biochimica e Biologia Molecolare, Universitá di Parma, 43100, Parma, Italy*

† Electronic supplementary information (ESI) available. See DOI: 10.1039/c1ob05433c

‡ Present address: Dipartimento di Fisica, Universitá di Modena, 41125 Modena, Italy; S3 Center CNR-NANO, 41125 Modena, Italy

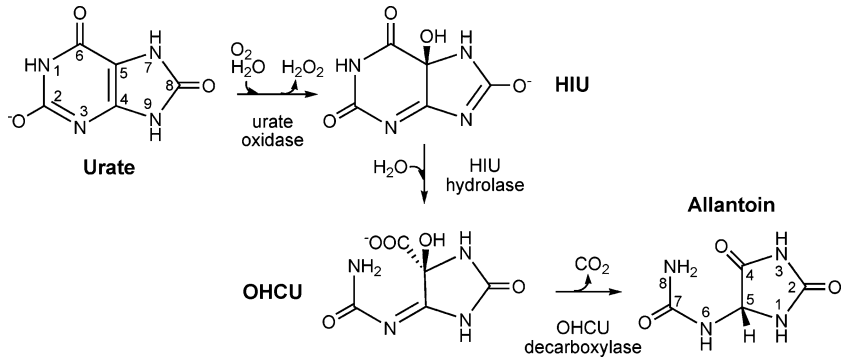

Scheme 1 The mammalian urate degradation pathway. HIU and OHCU isomers are drawn according to the results presented in this work.

produced during purine catabolism has already been proposed, with the assignment of the *S* configuration to the (+) enantiomer based on CD spectra comparison.[5] Although this assignment has never been called into question in the literature,[1,6,7] no direct crystallographic evidence is available. Recently, specific ^{13}C-labeling of allantoin, and NMR monitoring of the reaction catalyzed by allantoate amidohydrolase, an enzyme with known stereospecificity, have provided support to this assignment.[8] The intermediate species (HIU, OHCU) of the urate degradation pathway are unstable and establishing their absolute configuration is a challenge.

Recent developments in computational methods based on the time-dependent density functional theory (TDDFT)[9] for the calculation of chiroptical properties such as optical rotatory dispersion (ORD) and electronic circular dichroism (ECD) have increased their reliability to determine the absolute configuration of chiral molecules *in vitro*.[10–13] The absolute configuration is then assigned on the basis of the agreement between both computed and experimentally measured ORD and ECD spectra. In principle, results from only ORD or only ECD may be used for the assignment of the absolute configuration, however the assignment of absolute configuration is more robust when consistent results are obtained with both methods. Usually, one looks for a semi-quantitative agreement, as quantitative differences may be introduced by the limits of TDDFT inherent to the choice of the density functional/basis set, and from the non-consideration of the solvent effects on both conformational flexibility and on the molecular electronic responsive properties (*i.e.* rotational strengths and excitation energies[14,15]) determining the ORD and ECD spectra.

Solvent effects may be introduced by using the Polarizable Continuum Model (PCM),[16] in which the molecular solute treated at Quantum Mechanical (QM) level is placed in a cavity within the solvent represented as a dielectric medium characterized by its dielectric permittivity. Within the PCM framework, the ORD and ECD spectra of the chiral solutes may be computed considering both the solvent effect on the conformational equilibrium and both the effects on rotational strengths and excitation energies by exploiting the specific formulation of the TDDFT developed for PCM methods.[17,18] The TDDFT-PCM scheme provides a good picture of the ORD and ECD phenomena in solution,[19–23] and we exploit this methodology in order to assign absolute configurations of HIU, OHCU and allantoin within the urate degradation.

2 Experimental and computational procedures

Approximate ECD spectra of HIU, OHCU, and allantoin in the 200–350 nm range have been reported previously.[2] For the purpose of this work, accurate ECD spectra of the enzymatic products of urate degradation were collected in the 190–550 nm range. ECD measurements were carried out in a 10 mm pathlength cuvette with a Jasco J715 spectropolarimeter; data were collected at 0.5 nm intervals in 1 ml solution of 20 mM potassium phosphate, pH 7.6. HIU, OHCU, and allantoin were generated enzymatically from urate (0.1 mM) using 0.1 g of urate oxidase from *Candida utilis* (Sigma), plus 0.022 g of recombinant HIU hydrolase from zebrafish (for OHCU, allantoin), plus 0.17 g of recombinant OHCU decarboxylase from zebrafish (for allantoin). The experimental ORD spectra were obtained as Kramers-Kronig (KK) transform of the measured ECD spectra using the utility implemented in the Jasco Spectra Manager Software.

Theoretical simulations of chiro-optical properties (ECD and ORD) were carried out as the weighted sum of the computed chiro-optical responses $P_i(\nu)$ of the various isomers present in solution:

$$P(\nu) = \sum_{i=1}^{n} x_i P_i(\nu) \quad (1)$$

where x_i is the fractional population of the i^{th} isomer. The chiro-optical responses $P_i(\nu)$ (*i.e.* the specific rotation $[\alpha_i(\nu)]$ for ORD and the differential dichroic absorption $\Delta\varepsilon_i(\nu)$ for ECD) were computed using the TDDFT theory, and the effects of the solvent are treated using PCM formalism.

All the studied systems present in solution amino–imino tautomerism and/or conformational mobility (OHCU and allantoin). The corresponding molecular structures were determined by a systematic computational procedure at the DFT/B3LYP[24,25] level using the 6-31G** basis set[26] with the Polarizable Continuum Model (PCM) for solvation. In this procedure, the tautomeric species were selected from the most stable tautomers, within a window of 10 kcal/mol, of the various amino–imino forms in the gas phase. The equilibrium geometries of the selected tautomers were optimized in solution at the PCM/B3LYP/6-31G** level. For the selected tautomers of OHCU and allantoin a conformational analysis was performed, at the same level of theory, using both scan-relaxed and simple-scan procedures[27] in order to locate stable conformers as minima of the corresponding molecular potential energy surface. All the resulting minimum structures were

 This journal is © The Royal Society of Chemistry 2011

re-optimized without constraints, and confirmed as stable structures by the analysis of the Hessian matrix. The fractional populations of all the molecular species in solution (tautomers/conformers) were calculated with a Boltzmann approach:

$$x_i = \frac{e^{-\Delta G_{1,i}/RT}}{\sum_{i=1}^{n} e^{-\Delta G_{1,i}/RT}} \quad (2)$$

where $\Delta G_{1,i}$ is the standard free energy of the i-th conformer, relative to the most stable conformer (denoted by 1), and it is evaluated as

$$\Delta G_{1,i} = G_i - G_1 \quad (3)$$

where G_i is the standard free energy of the i-th conformer in solution, relative to a reference state given by non-interacting electrons and nuclei and by the unperturbed solvent. The standard free energy $G_{1,i}$ for each species was computed as the sum of the standard free energy in solution at 0 K, the unscaled zero point energy and the change of the free energy from 0 to 298 K. For each conformer, the standard free energy in solution at 0 K has been evaluated using the PCM/B3LYP theory and the AUG-cc-pVDZ[28] basis set. The zero-point energies and the thermal contributions were computed using the PCM/B3LYP theory with the 6-31G** basis set. In all the optimization and free-energy calculations in solution phase we employed the PCM model using the integral equation formulation (IEF-PCM),[29] with a solvent excluding surface cavity model[16] and UFF atomic radii[30] with scaling factor $\alpha = 1$.[31]

The single point calculations of the chiro-optical properties of the various species in solution were computed using the PCM-TDDFT theory in a non-equilibrium framework[16] with the AUG-cc-pVDZ basis set using two different exchange-correlation functionals, B3LYP and CAM-B3LYP.[32] Only species with relative population values higher than 5% were considered. The choice of the two different functionals is justified by the fact that the CAM-B3LYP functional is found to be particularly promising for the description of Rydberg-type electronic states that are frequently involved in the electronic transitions of the studied chromophores.[33] In all the single point PCM-TDDFT calculations we employed the scaling factors α of the UFF atomic radii optimized in a previous work on a set of molecular systems similar[34] to that considered in this work. The optimized scaling factors α are 0.91 for neutral species and 0.83 for anions. In the present work the solvent effect on the rotational strengths and on the optical rotations due to the local field correction were not considered.[35]

Optical rotations were calculated using a gauge-invariant formalism (GIAO).[36] Rotational strengths were computed by means of both length and velocity formalisms, to check *a posteriori* the degree of gauge-invariance. In all cases the rotational strengths obtained with the two formalisms do not differ significantly, so we only report the results for the length formalism.

The simulated ECD spectra were than obtained by superposition of Gaussian functions centered on each absorption wavelength (λ_{0i}):

$$\Delta\varepsilon(\lambda) = \frac{1}{2.294\times10^{-39}} \frac{1}{\sigma_\lambda\sqrt{2\pi}} \sum_i \lambda_{0i} R_{0i} e^{[-(\lambda-\lambda_{0i})^2/2\sigma_\lambda^2]} \quad (4)$$

where (σ_λ) is the half-height width of the gaussian function (set to 0.25 eV), the rotatory strengths, R_{0i}, are expressed in 10^{-40} esu^2 cm^2 and the differential absorption molar coefficient, $\Delta\varepsilon$, is expressed in L mol^{-1} cm^{-1}.

All the calculations were carried out with a development version of the Gaussian package.[31] The atomic coordinates of the equilibrium geometries and the computed rotatory strengths are reported in the ESI.†

3 Results and discussions

3.1 Tautomerism and conformational analysis

A critical issue for exploring the chiro-optical properties of enantiomers in solution is to obtain a careful description of the different tautomers and conformers that may be present in solution under the experimental conditions. The Boltzmann population of the different chemical species in solution has been computed using the density functional theory with a polarizable continuum model for solvation (See eqn (2) of Computational Procedures).

3.1.1 HIU isomers. Under the experimental conditions (pH = 7.6) HIU is present as a monoanionic species (see Schemes S1, S2 and Table S1 in the ESI† for details of the pK_a calculations) which may present tautomerism due to proton transfer.[37,38] In order to obtain a systematic description of the tautomeric structures of HIU, a tri-anionic species (see Scheme S3 in the ESI†) was chosen as the starting point, and from the analysis of its molecular electrostatic potential function computed at the B3LYP/6-31G** level 19 tautomers were selected. Their equilibrium geometries were computed in the gas phase, and finally, the five most stable structures were optimized in solution and considered for study of the fractional tautomeric populations in solution.

The values of free energy differences show a full predominance of the $HIU^{7,1}$ isomer (Fig. 1). On the basis of these fractional populations (Table 1) only the $HIU^{7,1}$ isomer was considered in the calculations of the ECD and ORD spectra of HIU.

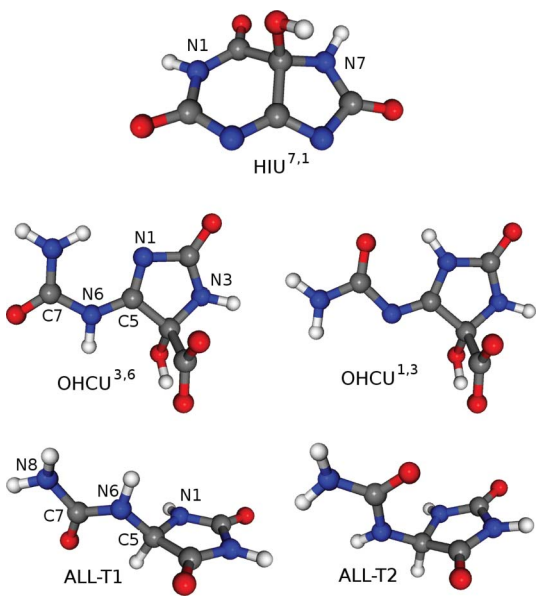

Fig. 1 $HIU^{7,1}$, $OHCU^{3,6}$, $OHCU^{1,3}$, ALL-T1, ALL-T2, *S* isomers. Atomic coordinates are available in the ESI.†

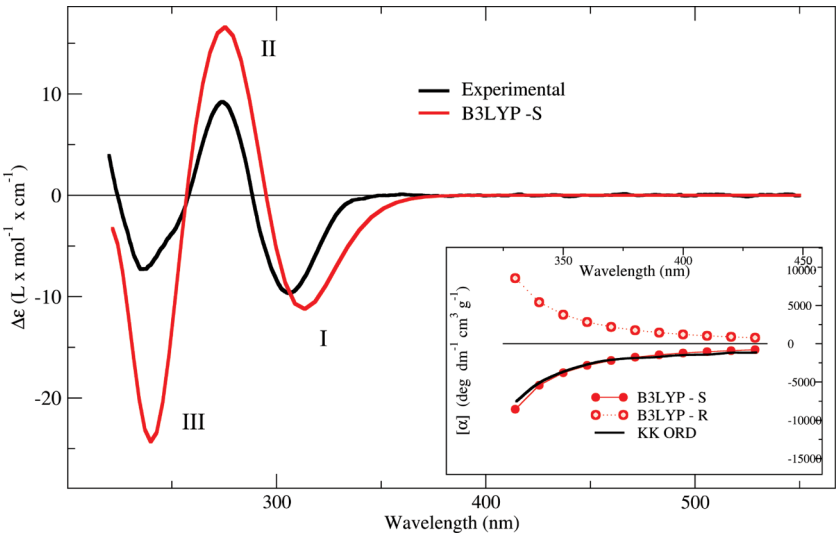

Fig. 2 Experimental and computed HIU spectra. Computed spectra (red) for the *HIU*[7,1] isomer were calculated at the PCM/TDDFT/B3LYP level. ORD spectra are shown in the inset. Red solid and red dotted lines refer to the *S* and *R* configurations of *HIU*[7,1], respectively.

Table 1 Gibbs free energy differences in kcal mol^{-1} and relative populations of HIU, OHCU and allantoin isomers in solution

	HIU[7,1]	OHCU[1,3]	OHCU[3,6]	ALL-T1	ALL-T2
ΔG	0.0	0.0	0.2	0.0	7.1
x_i	1.00	0.57	0.43	0.93	0.05

3.1.2 OHCU isomers. The OHCU monoanions exhibits both proton tautomerism and conformational flexibility.[37,38] The tautomeric forms were selected by a procedure similar to that used for HIU. Starting from a tri-anionic species (see Scheme S3 in the ESI†), six protonation sites were located and 13 tautomers were initially selected. Their equilibrium geometries were first computed in the gas phase, then optimized in solution and finally the two most stable structures, denoted as *OHCU*[1,3] and *OHCU*[3,6], were considered for the study of optical properties in solution. The two tautomers present conformational flexibility with respect to the torsion angles involving atoms N1C5N6C7 and C5N6C7N8, respectively (Fig. 1).

Eight stable conformers in solution were first determined as minima of the potential energy surface scanned along these two conformational degrees of freedom.§ All the eight conformers were confirmed as true minima of the PES by complete optimization of their geometries. The values of free energy difference and the corresponding fractional populations are reported in Table 1 only for the two conformers that have significant fractional populations.

The data show a slight prevalence of the most stable conformer of the tautomeric form *OHCU*[1,3] over the most stable conformer of taumeric form *OHCU*[6,3]. These two conformers were considered in the calculations of the ECD and ORD spectra of OHCU in solution.

3.1.3. Allantoin isomers. Allantoin (pK_a = 8.96) is a neutral species in aqueous solutions under the experimental conditions, and presents a complex conformational flexibility. From preliminary B3LYP/6-31G** calculations in the gas phase only a chemically relevant tautomer was obtained. This tautomeric form is characterized by a high conformational flexibility, as also noted in a previous *ab initio* HF study on allantoin,[6] due to the torsion angles involving atoms C5N6C7N8 and N1C5N6C7, respectively (Fig. 1).

By exploiting a scan-relaxed procedure six low energy conformers are located in the gas phase and all of them were considered for the study in solution. The fractional populations of the dominant conformers are reported in Table 1. The ALL-T1 conformer is found to be the predominant species in aqueous solutions, but ALL-T2 shows a significant, although numerically small, population. Therefore, the chiro-optical properties of allantoin were computed considering the presence of these two conformers.

3.2 ECD and ORD spectra and absolute configuration assignments

In the following sections we present the computed ORD and ECD spectra of HIU, OHCU, and allantoin in order to obtain an assignment of the absolute configuration of the species generated by the enzymatic degradation of urate (see Fig. 1) by comparison with the experimental spectra.

3.2.1 HIU spectra. In Fig. 2, the B3LYP theoretical ECD and ORD spectra of the *S* stereoisomer of the *HIU*[7,1] tautomer are compared with the experimental data.

The experimental ECD spectrum of HIU shows a negative peak (I) centered around 308 nm, a positive peak (II) centered around 275 nm and a negative peak (III) around 235 nm. The experimental ORD curve presents negative rotation in the spectral range considered (350–465 nm). The computed ECD spectrum gives a good reproduction of the absorption wavelengths and intensities related to the three experimental peaks. The experimental negative rotation is also well reproduced by the theoretical ORD curve.

The CAM-B3LYP results show a similar behaviour (see ESI,† Figure S1), with a systematic shift toward shorter wavelengths

§ A step size of 18° was chosen for both the torsion angles, and a total of 400 PES points have been collected.

This journal is © The Royal Society of Chemistry 2011

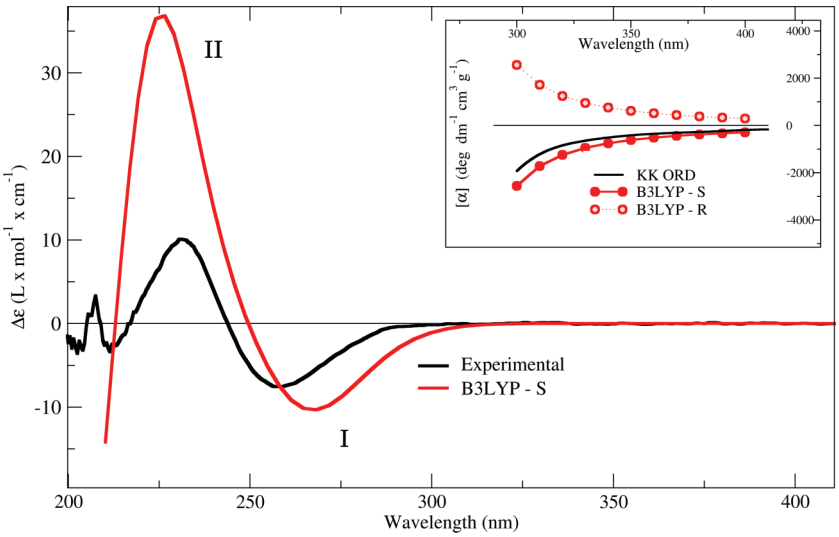

Fig. 3 Experimental and computed OHCU spectra. Computed spectra (red) for the Boltzmann population of *OHCU*[1,3] and *OHCU*[6,3] isomers, were calculated at the PCM/TDDFT/B3LYP level. ORD spectra are shown in the inset. Red solid and red dotted lines refer to the *S* and *R* configurations of the OHCU isomers, respectively.

in the ECD spectrum, and a systematic underestimation of the optical rotation signal in the ORD spectrum.

On the basis of the good agreement between the computed spectra and the experimental data we assign the *S* configuration to the (–)-HIU intermediate generated by the enzymatic degradation of urate.

3.2.2 OHCU spectra. In Fig. 3, the B3LYP computed ECD and ORD spectra of the Boltzmann distribution of *OHCU*[1,3] and *OHCU*[6,3] tautomers in the *S* configuration, are compared with the experimental data. The corresponding spectra for the single tautomers are reported in Figure S4 of the ESI.†

The experimental ECD spectrum of OHCU presents as major signatures a negative peak (I) centered around 257 nm, and a positive peak (II) centered around 230 nm. The experimental ORD curve presents negative rotation in the spectral range considered (300–400 nm). The computed ECD spectrum gives a good reproduction of the absorption wavelengths and intensities of the two experimental peaks. The experimental negative rotation is also well reproduced by the theoretical ORD curve.

The CAM-B3LYP results show a similar behaviour (see ESI,† Figure S3), with a systematic shift toward shorter wavelengths in the ECD spectrum, and a systematic underestimation of the optical rotation signal in the ORD spectrum.

On the basis of the good agreement between the computed spectra and the experimental data, we assign the *S* configuration to the (–)-OHCU intermediate generated by the enzymatic degradation of urate.

3.2.3 Allantoin spectra. In Fig. 4, the computed B3LYP ECD and ORD spectra of the Boltzmann distribution of ALL-T1 and ALL-T2 conformers of allantoin in the *S* configuration are compared with the experimental data. The corresponding spectra for the single tautomers are reported in Figure S4 of the ESI.†

The experimental ECD spectrum of allantoin presents as major signatures a weak broad negative peak (I) around 240 nm, and strong positive peak (II) centered at 208 nm. The experimental ORD curve presents a positive rotation in all the spectral range considered (250–400 nm).

The B3LYP computed ECD spectrum of (*S*)-allantoin is consistent with the sign of the band II, but not with the sign of the weak band I. The corresponding CAM-B3LYP spectrum (see ESI,† Figure S5) shows a similar behaviour. However, both the B3LYP and CAM-B3LYP calculated ORD spectra of (*S*)-allantoin (see Fig. 3 and Figure S5) are in agreement with the experimentally observed positive rotation in the spectral region from 250 nm to 400 nm.

Although the TDDFT-ECD results cannot provide conclusive evidence on the absolute configuration of allantoin stereoisomers, the agreement between the computed and experimental ORD spectra supports the previous assignment of the *S* configuration to (+)-allantoin.[5,40]

4 Concluding remarks

The TDDFT-PCM computed chiro-optical ECD and ORD spectra for HIU and OHCU species are in good agreement with the corresponding experimentally measured spectra. This agreement leads to a non-ambiguous assignment for both intermediates HIU and OHCU to the (–)-*S* configuration. Given that the formation of OHCU through the hydrolysis of HIU does not change the configuration at the chiral center (see Scheme 1), the independent assignment of the same configuration to HIU and OHCU gives further support to the proposed stereochemistry (the same reasoning does not apply to allantoin, in which a different chiral center is involved).

The TDDFT-PCM computed ORD and ECD spectra for allantoin reproduce the main features of the experimentally measured spectra, confirming the (+)-*S* configuration in agreement with the previous assignments based on CD experimental measurements and biochemical evidence. Some minor features of the computed ECD spectra in the long-wavelength region do not agree in sign with the experimental ECD spectra, due to the limitations

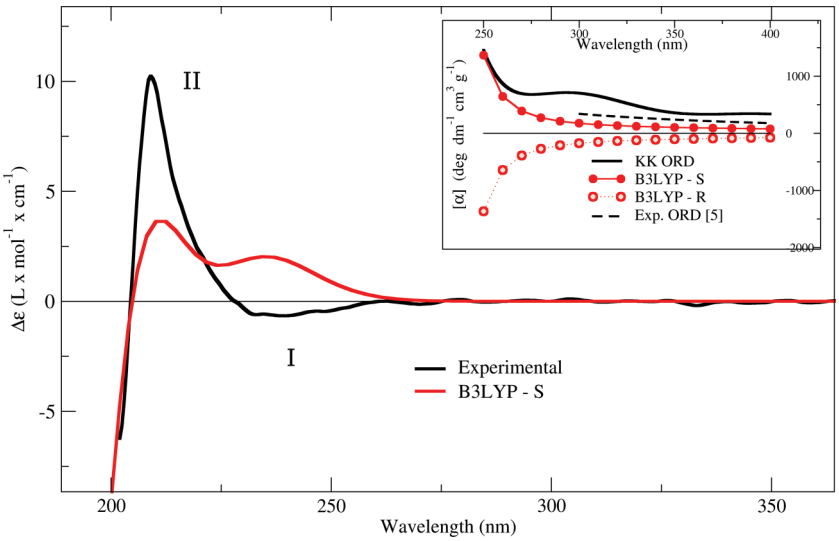

Fig. 4 Experimental and computed allantoin spectra. Computed spectra (red) for the Boltzmann distribution of ALL-T1 and ALL-T2 isomers were calculated at the PCM/TDDFT/B3LYP level. ORD spectra are shown in the inset. Red solid and red dotted lines refer to the *S* and *R* configurations of the allantoin isomers, respectively; the black dashed line shows experimental data of (+)-allantoin from Ref. 5.

of the TDDFT-PCM method. However, it is well known that given the actual TDDFT technology one should not expect for the computation of ECD spectra the same reliability of the computations of ORD spectra in the assignment of absolute configurations.[39]

Although the stereochemistry of urate degradation has not been directly investigated in crystallographic studies, previous evidence obtained by the structural analysis of the enzymes involved in the metabolic pathway is consistent with our results. Detailed investigations of the urate oxidase structure in complex with inhibitors have localized a water molecule candidate for the hydroxylation step of the reaction near to the si-face of urate, thus suggesting formation of (*S*)-HIU.[41,42] Docking of the unstable substrate at the active site of OHCU decarboxylase has suggested binding of the *S* enantiomer of OHCU and has localized a histidine residue candidate for catalysis in a position consistent with the formation of (*S*)-allantoin.[43–45]

The information on the absolute stereochemistry and preferred conformations of urate oxidation products obtained in this work through theoretical calculations and comparison with experimental spectra could prove useful for the study of the catalytic mechanism of the enzymes involved in the metabolic pathway, and for the understanding of the molecular basis of the toxicity of the unstable intermediates of urate degradation.

Abbreviations

HIU	5-hydroxyisourate
OHCU	2-oxo-4-hydroxy-4-carboxy-5-ureidoimidazoline
QM	quantum mechanical
PCM	polarizable continuum model
IEF	integral equation formalism
ECD	electronic circular dichroism
ORD	optical rotatory dispersion
DFT	density functional theory
TDDFT	time-dependent density functional theory
GIAO	gauge invariant atomic orbitals

Acknowledgements

We thank Vincenzo Puggioni for help with CD measurements. This work has been supported by the University of Parma.

References

1 P. A. Tipton, *Nat. Chem. Biol.*, 2006, **3**, 124–125.
2 I. Ramazzina, C. Folli, A. Secchi, R. Berni and R. Percudani, *Nat. Chem. Biol.*, 2006, **2**, 144–148.
3 R. Terkeltaub, *Nat. Rev. Rheumatol.*, 2010, **6**, 30–38.
4 W. S. Stevenson, C. D. Hyland, J. G. Zhang, P. O. Morgan, T. A. Willson, A. Gill, A. A. Hilton, E. M. Viney, M. Bahlo, S. L. Masters, S. Hennebry, S. J. Richardson, N. A. Nicola, D. Metcalf, D. J. Hilton, A. W. Roberts and W. S. Alexander, *Proc. Natl. Acad. Sci. U. S. A.*, 2010, **107**, 16625–16630.
5 E. J. Gravenmade, G. D. Vogels and C. van Pelt, *Recl. Trav. Chim. Pays-Bas*, 1969, **88**, 929–939.
6 K. Kahn and P. A. Tipton, *Bioorg. Chem.*, 2000, **28**, 62–72.
7 I. Ramazzina, L. Cendron, C. Folli, R. Berni, D. Monteverdi, G. Zanotti and R. Percudani, *J. Biol. Chem.*, 2008, **283**, 23295–23304.
8 F. Serventi, I. Ramazzina, I. Lamberto, V. Puggioni, R. Gatti and R. Percudani, *ACS Chem. Biol.*, 2010, **5**, 203–214.
9 E. Runge and E. K. U. Gross, *Phys. Rev. Lett.*, 1984, **52**, 997–1000.
10 P. J. Stephens, F. J. Devlin, J. R. Cheeseman and M. J. Frisch, *J. Phys. Chem. A*, 2001, **105**, 5356–5371.
11 P. J. Stephens, F. J. Devlin, J. R. Cheeseman and M. J. Frisch, *Chirality*, 2002, **14**, 288–296.
12 P. J. Stephens, F. J. Devlin, J. R. Cheeseman, M. J. Frisch, O. Bortolini and P. Besse, *Chirality*, 2003, **15**, S57–S64.
13 P. Polavarapu, *Chirality*, 2008, **20**, 664–672.
14 L. Rosenfeld, *Z. Phys.*, 1928, **52**, 161–174.
15 D. J. Caldwell and H. Eyring, *The Theory of Optical Activity*, Wiley, 1971.
16 J. Tomasi, B. Mennucci and R. Cammi, *Chem. Rev.*, 2005, **105**, 2999–3094.
17 R. Cammi, B. Mennucci and J. Tomasi, *J. Phys. Chem. A*, 2000, **104**, 5631–5637.
18 M. Cossi and V. Barone, *J. Chem. Phys.*, 2001, **115**, 4708–4717.

 This journal is © The Royal Society of Chemistry 2011

19 P. J. Stephens, F. J. Devlin, J. R. Cheeseman, M. J. Frisch, B. Mennucci and J. Tomasi, *Tetrahedron: Asymmetry*, 2000, **11**, 2443–2448.
20 B. Mennucci, J. Tomasi, R. Cammi, J. R. Cheeseman, M. J. Frisch, F. J. Devlin and P. J. Stephens, *J. Phys. Chem. A*, 2002, **106**, 6102–6113.
21 C. O. da Silva, B. Mennucci and T. Vreven, *J. Org. Chem.*, 2004, **69**, 8161–8164.
22 D. Marchesan, S. Coriani, C. Forzato, P. Nitti, G. Pitacco and K. Ruud, *J. Phys. Chem. A*, 2005, **109**, 1449–1453.
23 S. Coriani, A. Baranowska, L. Ferrighi, C. Forzato, D. Marchesan, P. Nitti, G. Pitacco, A. Rizzo and K. Ruud, *Chirality*, 2006, **18**, 357–369.
24 A. D. Becke, *J. Chem. Phys.*, 1993, **98**, 5648–5652.
25 C. Lee, W. Yang and R. G. Parr, *Phys. Rev. B*, 1988, **37**, 785–789.
26 R. Ditchfield, W. J. Hehre and J. A. Pople, *J. Chem. Phys.*, 1971, **54**, 724–728.
27 J. B. Foresman and A. Frisch, *Exploring Chemistry with Electronic Structure Methods*, Gaussian, Inc., 1993.
28 Jr. T. H. Dunning, Gaussian basis sets for use in correlated molecular calculations. I. The atoms boron through neon and hydrogen, *J. Chem. Phys.*, 1989, **90**, 1007–1024.
29 E. Cances, B. Mennucci and J. Tomasi, *J. Chem. Phys.*, 1997, **107**, 3032–3042.
30 K. A. Rappe, C. J. Casewit, K. S. Colwell, W. A. Goddard and M. W. Skiff, *J. Am. Chem. Soc.*, 1992, **114**, 10024–10035.
31 *Gaussian Development Version, Revision G.03*, M. J. Frisch, G. W. Trucks, H. B. Schlegel, G. E. Scuseria, M. A. Robb, J. R. Cheeseman, J. A. Montgomery, Jr., T. Vreven, G. Scalmani, B. Mennucci, V. Barone, G. A. Petersson, M. Caricato, H. Nakatsuji, M. Hada, M. Ehara, K. Toyota, R. Fukuda, J. Hasegawa, M. Ishida, T. Nakajima, Y. Honda, O. Kitao, H. Nakai, X. Li, H. P. Hratchian, J. E. Peralta, A. F. Izmaylov, K. N. Kudin, J. J. Heyd, E. Brothers, V. N. Staroverov, G. Zheng, R. Kobayashi, J. Normand, J. L. Sonnenberg, F. Ogliaro, M. Bearpark, P. V. Parandekar, G. A. Ferguson, N. J. Mayhall, S. S. Iyengar, J. Tomasi, M. Cossi, N. Rega, J. C. Burant, J. M. Millam, M. Klene, J. E. Knox, J. B. Cross, V. Bakken, C. Adamo, J. Jaramillo, R. Gomperts, R. E. Stratmann, O. Yazyev, A. J. Austin, R. Cammi, C. Pomelli, J. W. Ochterski, P. Y. Ayala, K. Morokuma, G. A. Voth, P. Salvador, J. J. Dannenberg, V. G. Zakrzewski, S. Dapprich, A. D. Daniels, M. C. Strain, O. Farkas, D. K. Malick, A. D. Rabuck, K. Raghavachari, J. B. Foresman, J. V. Ortiz, Q. Cui, A. G. Baboul, S. Clifford, J. Cioslowski, B. B. Stefanov, G. Liu, A. Liashenko, P. Piskorz, I. Komaromi, R. L. Martin, D. J. Fox, T. Keith, M. A. Al-Laham, C. Y. Peng, A. Nanayakkara, M. Challacombe, W. Chen, M. W. Wong, and J. A. Pople, Gaussian, Inc., Wallingford CT, 2007.
32 T. Yanai, D. Tew and N. Handy, *Chem. Phys. Lett.*, 2004, **393**, 51–57.
33 M. J. G. Peach, P. Benfield, T. Helgaker and D. J. Tozer, *J. Chem. Phys.*, 2008, **128**, 044118–044126.
34 V. Verdolino, R. Cammi, B. H. Munk and H. B. Schlegel, *J. Phys. Chem. B*, 2008, **112**, 16860–16873.
35 S. Pipolo, R. Cammi, A. Rizzo, C. Cappelli, B. Mennucci and J. Tomasi, *Int. J. Quantum Chem.*, 2011, **111**, 826–838.
36 R. Ditchfield, *Mol. Phys.*, 1974, **27**, 789–807.
37 K. Kahn, P. Serfozo and P. A. Tipton, *J. Am. Chem. Soc.*, 1997, **119**, 5435–5442.
38 K. Kahn and P. A. Tipton, *Biochemistry*, 1998, **37**, 11651–11659.
39 D. M. McCann and P. J. Stephens, *J. Org. Chem.*, 2006, **71**, 6074–6098.
40 S. Ding, A. Kolbanowskiy, A. Durandin, C. Crean, V. Shafirovich, S. Broyde and N. E. Geacintov, *Chirality*, 2009, **21**, E231–E241.
41 L. Gabison, M. Chiadmi, N. Colloc'h, B. Castro, M. El Hajji and T. Prang, *FEBS Lett.*, 2006, **580**, 2087–2091.
42 N. Colloc'h, L. Gabison, G. Monard, M. Altarsha, M. Chiadmi,G. Marassio, J. Sopkova-de Oliveira Santos, M. El Hajji, B. Castro, J. H. Abraini and T. Prang, *Biophys. J.*, 2008, **95**, 2415–2422.
43 L. Cendron, R. Berni, C. Folli, I. Ramazzina, R. Percudani and G. Zanotti, *J. Biol. Chem.*, 2007, **282**, 18182–18189.
44 K. Kim, J. Park and S. Rhee, *J. Biol. Chem.*, 2007, **282**, 23457–23464.
45 J. B. French and S. E. Ealick, *J. Biol. Chem.*, 2010, **285**, 35446–35454.